International Journal of Vehicle Design

ISSN online: 1741-5314 - ISSN print: 0143-3369
https://www.inderscience.com/ijvd

Refined modelling of thin-walled beam, plate and joint for automobile frame

Jiantao Bai, Wenjie Zuo

DOI: 10.1504/IJVD.2023.10058870

Article History:

Received:	21 April 2017
Last revised:	29 May 2020
Accepted:	13 June 2020
Published online:	04 September 2023

Refined modelling of thin-walled beam, plate and joint for automobile frame

Jiantao Bai and Wenjie Zuo*

School of Mechanical and Aerospace Engineering,
Jilin University,
Changchun, 130025, China
Email: baijiantao@jlu.edu.cn
Email: zuowenjie@jlu.edu.cn
*Corresponding author

Abstract: At the conceptual design stage, the simplified frame is extensively applied in the body-in-white (BIW) structure to rapidly calculate its performances. However, it is difficult to acquire an accurate simplified frame of the BIW structure for the calculation of the bending stiffness, torsional stiffness and frequencies. Therefore, this paper proposes a simplified modelling method by using the thin-walled beams (TWBs) with complex sections, semi-rigid elements and cross beam structures. Compared with the traditional modelling method, the TWBs contain more types of the complex sections, the semi-rigid elements are used to describe various deformations, and the plate structure is replaced by using the cross beam structure to improve the accuracy of the simplified frame. An engineering example demonstrates that the simplified frame can accelerate the conceptual design of the BIW structure.

Keywords: conceptual design; frame structure; complex section; semi-rigid element; cross beam structure.

Reference to this paper should be made as follows: Bai, J. and Zuo, W. (2023) 'Refined modelling of thin-walled beam, plate and joint for automobile frame', *Int. J. Vehicle Design*, Vol. 92, No. 1, pp.22–41.

Biographical notes: Jiantao Bai received his BS, MS, and PhD from the Jilin University in 2014, 2017 and 2021, respectively. Currently, he is a post-Doctor in Jilin University. His research fields include structural optimisation and CAE software development.

Wenjie Zuo received his BS, MS, and PhD from the Jilin University in 2005, 2007 and 2010, respectively. Currently, he is a Professor in Jilin University. His research fields include structural optimisation and CAE software development.

1 Introduction

The design of the automobile structure mainly undergoes two stages, i.e., conceptual design and detailed design. At the conceptual design stage, it is important to rapidly and accurately evaluate the performances of the automobile structure, which can greatly shorten design period and reduce manufacturing risk (Nishigaki et al., 2001; Zuo, 2015). Especially, to facilitate the development of new production, the demand of the conceptual design for many automobile manufacturers continues to increase (Hou et al., 2015; Zuo et al., 2011).

Since the body-in-white (BIW) structure is the important load-bearing structure and occupies about one third of the total mass of the whole automobile, it has been extensively studied (Overhagh, 1995). Many methods have been put forward to conceptually design the BIW structure. Among these methods, the simplified frame consisting of beam elements is widely employed to design the BIW structure, which is composed of many types of the complex sections. Therefore, many researchers applied the computer-aided-design software to design the cross-sectional shapes of the BIW structure (Huang et al., 2011, 2015; Wang et al., 2010). Also, much effort has been devoted to establish the simplified frame, for example, the first order analysis (FOA) initially used the Microsoft Excel to design the complex sections, but only some types of the complex sections, i.e., open-, single- and double-cell, were applied to the simplified frame (Nishigaki et al., 2001, 2004). Nishigaki and Kikuchi (2004) focused on the crashworthiness of the FOA, and predicted the collapse behaviour of the simplified frame. Nakagawa et al. (2004) extended the FOA for the noise and vibration with the Euler's beam theory. The shape optimisation of the complex sections of the thin-walled beams (TWBs) was studied (Yoshimura et al., 2005), but three- and four-cell sections have not been considered. Then, Zuo et al. (2012) utilised the beam elements and semi-rigid elements to improve the accuracy of the simplified frame. Moreover, to improve the crashworthiness of the TWB, the genetic algorithm was employed to optimise the complex sections (Zuo and Bai, 2016; Bai et al., 2017). Besides, the reduced beam and joint modelling method was proposed by Donders et al. (2009) to design the BIW structure by considering the torsional stiffness, bending stiffness and modes, in which all the complex TWBs were simplified as rectangular tubes. Furthermore, component sensitivity analysis was proposed to modify and optimise the simplified frame with rectangular tubes (Chen and Zuo, 2014; Zuo and Saitou, 2017; Zuo et al., 2016). Torstenfelt and Klarbring (2007) adopted the size, shape and topology optimisation method to design and optimise the conceptual automobile product. Recently, Bai and Zuo (2020) employed the topology optimisation method to design the hollow structure, which can further promote the design of thin-walled structures. However, the above investigations did not mention the four-cell section, which is often applied in the B-Pillar structure.

Meanwhile, the joint structures are important parts of the BIW structure (Hou et al., 2011; Shahhosseini et al., 2010). Mostly, the simplified joint structure was regarded as spring elements, whose stiffness was obtained from the detailed finite element (FE) model or experimental test of the joint structure (Mundo et al., 2011; Nikolaidis and Lee, 1992; Suh et al., 2002). Actually, the joint structure is unavailable at the conceptual design stage. Therefore, the spring stiffness should be approximately calculated by using

the detailed FE model of the TWB at that stage. Among them, the beam elements and torsional spring elements are employed to create the simplified frame and evaluate the performances of the BIW structure (Lyu et al., 2006; Lyu and Saitou, 2006). However, the above investigations did not cover the axial collapse, shear, bending and torsional springs, which have a significant influence on the joint structure. Also, the plate structures, such as ceiling, floor and firewall, are also important load-bearing structures, but the degrees of freedom (DoFs) between the plate element and beam element are inconsistent, so the plate structures are usually omitted in the simplified frame (Hamza and Saitou, 2004; Mohsin and Sadek, 1980).

Therefore, in this paper a simplified modelling method is proposed to create the simplified frame by using the TWBs with complex sections, semi-rigid elements and cross beam structures, in which the properties of the complex sections are summarised and derived, the detailed FE model of the TWBs is employed to accurately and rapidly solve the spring stiffness, and the cross beam structure is introduced to replace the plate structure by the equivalence of the mass and central deflection for the first time. Finally, the performance evaluation of the simplified frame is conducted and compared with the benchmarking BIW structure.

2 Frame structure design

2.1 Simplified frame of the BIW structure

The BIW structure is composed of the TWB, plate and joint structures (Hou et al., 2011). The beam elements are used to create the simplified frame of the BIW structure (Zuo, 2015). Recently, Gui et al. (2018), Bai et al. (2019a, 2019b) employed the beam elements to create the simplified frame of the automobile and bus structures. Generally, the joint structures undergo greater deformation than the TWB structures under static or dynamic conditions. The semi-rigid elements with various spring elements are created between the beam elements to describe the large deformation. Traditionally, the spring stiffness was solved by using the detailed FE model of the joint structure (Zuo et al., 2012). But, the detailed FE model of the joint structure cannot be determined at the conceptual design stage, so the detailed FE model of the TWB structure is used to solve the spring stiffness in this paper, which can be accurately and rapidly solved by using this method. In addition, some plate structures have a great influence on the deformation of the whole BIW structure. The cross beam structure is introduced to describe the deformation of the plate structure for the first time. In this paper, the Yaris BIW structure is used to demonstrate the effectiveness of the proposed method. The detailed FE model is shown in Figure 1, which contains 232 components, 495000 shell elements and 1510000 DoFs. The simplified frame is shown in Figure 2, which contains 470 semi-rigid elements, 50 complex sections and 5600 DoFs. Compared with the detailed FE model, the simplified frame has less elements and DoFs, so the modelling and computational costs can be greatly reduced.

Figure 1 A detailed FE model of Yaris BIW (see online version for colours)

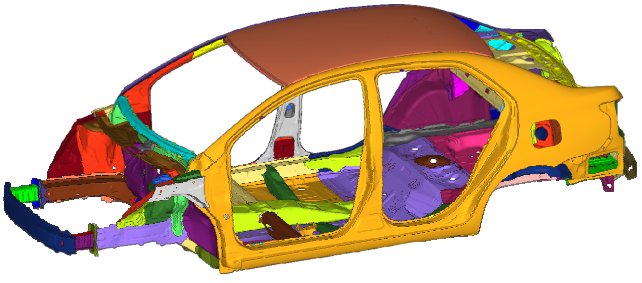

Figure 2 Simplified frame of Yaris BIW (see online version for colours)

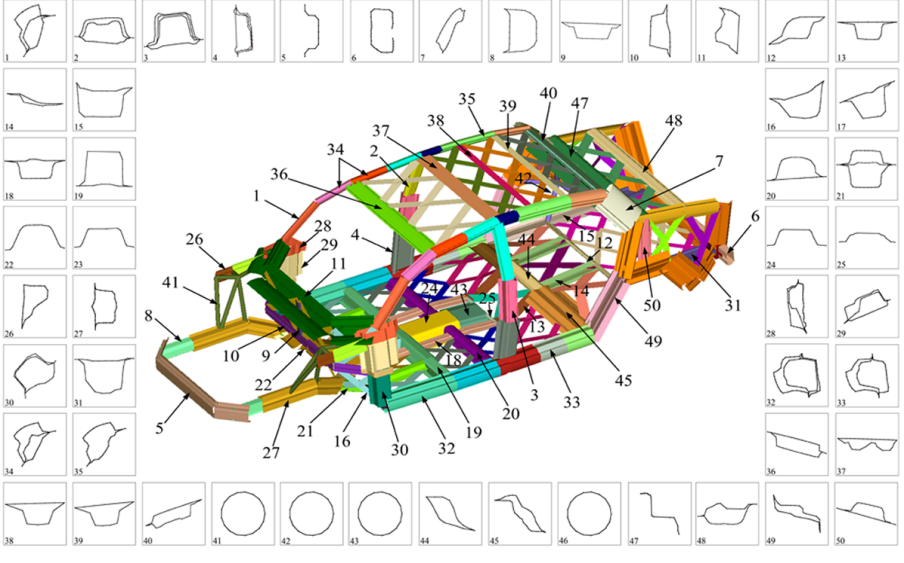

2.2 Simplified model of thin-walled beam

The beam elements with six DoFs, which can simulate each type of the deformations (Mundo et al., 2011), are usually used to simplify the TWBs of the BIW structure, since the simplified frame with less elements can be easily created and quickly solved by the parameterised modelling method. It is worth noting that the properties of the complex sections need to be accurately solved. The complex sections of the TWBs mainly include open-, single-, double-, three- and four-cell. Figure 3 shows a typical three-cell section. The properties of open-, single- and double-cell can be accurately calculated in current CAE software, such as HyperMesh and FOA. Zuo et al. (2018), Zuo and Bai (2016) and Bai et al. (2017) detailedly designed and optimised these complex sections. These studies demonstrate that their properties are greatly important. However, for an arbitrary multi-cell section, the torsional moment of inertia cannot be accurately obtained. Therefore, the properties of these complex sections are summarised. Especially, the torsional moments of inertia of the multi-cell sections are derived.

Figure 3 The demonstration for three-cell section (see online version for colours)

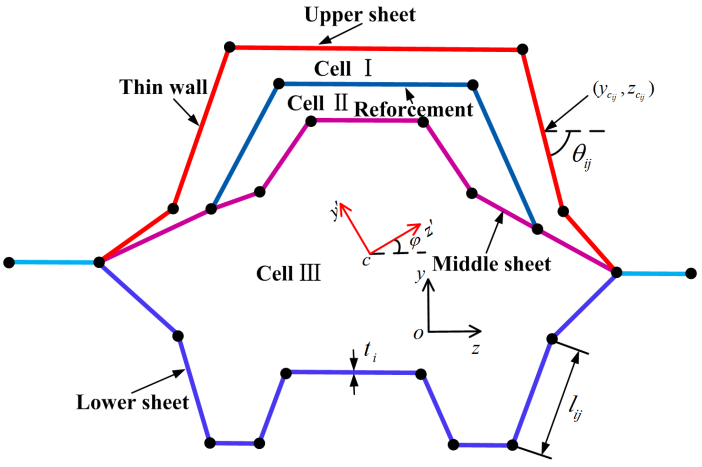

The complex section consists of some sheets, and each sheet is composed of some rectangle segments. So its area can be written as

$$A = \sum_{i=1}^{n}\sum_{j=1}^{m} A_{ij} = \sum_{i=1}^{n}\sum_{j=1}^{m} l_{ij} t_i \tag{1}$$

where n and m denote the number of the sheets and segments, respectively. t_i, l_{ij} and A_{ij} denote thickness, length and area of the segment, respectively.

The cross-sectional center can be expressed as

$$y_c = \frac{1}{A}\sum_{i}^{n}\sum_{j}^{m} A_{ij} y_{c_{ij}} \quad \text{and} \quad z_c = \frac{1}{A}\sum_{i}^{n}\sum_{j}^{m} A_{ij} z_{c_{ij}} \tag{2}$$

where $(y_{C_{ij}}, z_{C_{ij}})$ denotes the centre of the segment.

According to the elasticity theory (Timoshenko and Goodier, 1951), the moments of inertia I_y, I_z and product of inertia I_{yz} of an arbitrary complex section, as shown in Figure 4, can be respectively obtained by

$$\begin{cases} I_y = \int_A z^2 \mathrm{d}A \\ I_z = \int_A y^2 \mathrm{d}A \\ I_{yz} = \int_A yz \mathrm{d}A \end{cases} \tag{3}$$

I_y, I_z and I_{yz} can be respectively expressed as

$$I_y = \sum_{i=1}^{n}\sum_{j=1}^{m}\left[\left(\frac{l_{ij}t_i^3}{12}\right)\sin^2\theta_{ij} + \left(\frac{l_{ij}^3 t_i}{12}\right)\cos^2\theta_{ij} + l_{ij}t_i y_{C_{ij}}^2\right] \tag{4}$$

$$I_z = \sum_{i=1}^{n}\sum_{j=1}^{m}\left[\left(\frac{l_{ij}t_i^3}{12}\right)\cos^2\theta_{ij} + \left(\frac{l_{ij}^3 t_i}{12}\right)\sin^2\theta_{ij} + l_{ij}t_i z_{C_{ij}}^2\right] \tag{5}$$

$$I_{yz} = \sum_{i=1}^{n}\sum_{j=1}^{m}\left[\left(\frac{l_{ij}^3 t_i - l_{ij}t_i^3}{24}\right)\sin 2\theta_{ij} + l_{ij}t_i z_{C_{ij}} y_{C_{ij}}\right] \tag{6}$$

where θ_{ij} denotes angle between the z axis and segment. Furthermore, the principal moment of inertia can be obtained as

$$I_{\max} = \frac{1}{2}\left(I_y + I_z\right) + \sqrt{\frac{1}{2}\left(I_y - I_z\right)^2 + I_{yz}^2} \tag{7}$$

$$I_{\min} = \frac{1}{2}\left(I_y + I_z\right) - \sqrt{\frac{1}{2}\left(I_y - I_z\right)^2 + I_{yz}^2} \tag{8}$$

The following differential equation can be used to solve the torsional moment of inertia J

$$\begin{cases} \dfrac{\partial^2\phi}{\partial x^2} + \dfrac{\partial^2\phi}{\partial y^2} = -2G\theta \\ \phi_x = 0 \end{cases} \tag{9}$$

where $\phi(x, y)$ denotes stress function and θ denotes torsional angle. Then, J can be calculated as

$$J = M = 2\int_A \phi \mathrm{d}A \tag{10}$$

The calculation of J depends on the type of the complex section, as shown in Figure 5. For the open-cell, J° can be expressed as

$$J^{\circ} = \sum_{i=1}^{o}\sum_{j=1}^{m} l_{ij}t_i^3 \tag{11}$$

where o denotes the number of the sheets.

Figure 4 Arbitrary cross-sectional section (see online version for colours)

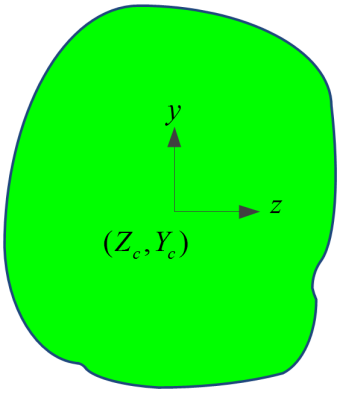

Figure 5 Five types of cross section (see online version for colours)

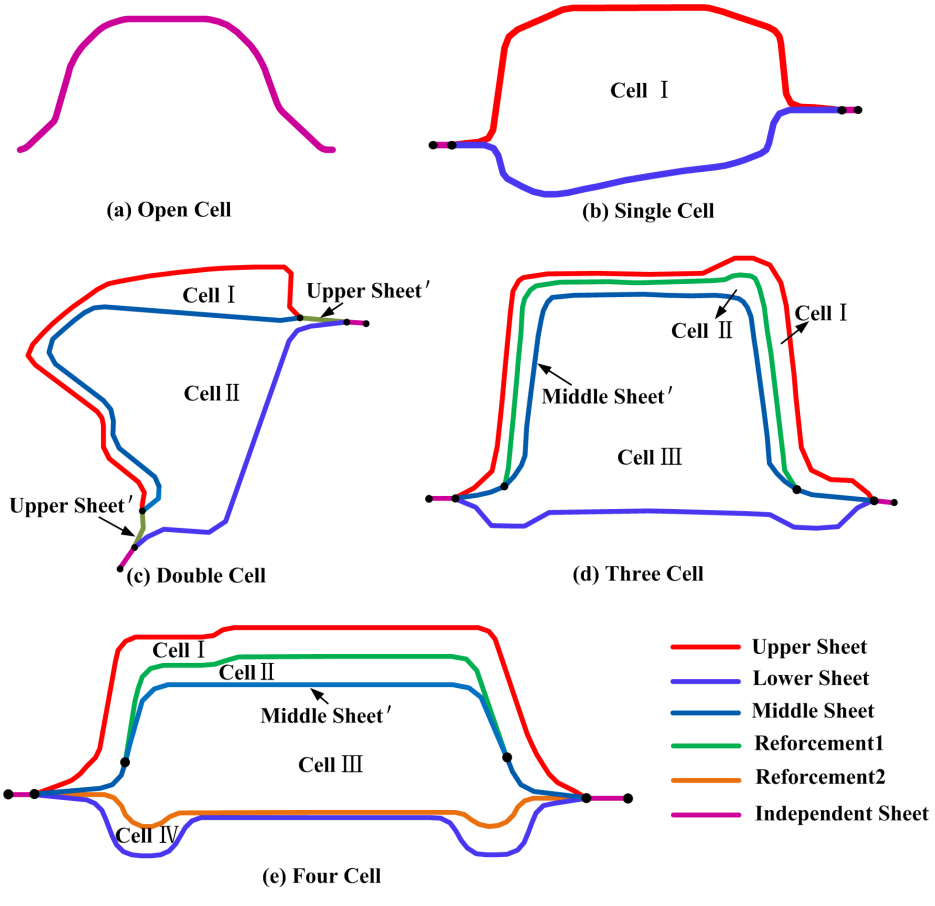

For the single-, double-, three- and four-cell, J_1^c, J_2^c, J_3^c and J_4^c can be further expressed as

$$J_1^c = \frac{4F_1^2}{L_l/t_l + L_u/t_u} \tag{12}$$

$$J_2^c = \frac{4\left\{F_1^2\left(\frac{L_l}{t_l}+\frac{L_r}{t_r}+\frac{L_u-L_u'}{t_u}\right)-F_2^2\left(\frac{L_r}{t_r}+\frac{L_u'}{t_u}\right)\right\}}{\left(\frac{L_r}{t_r}+\frac{L_u'}{t_u}\right)\left(\frac{L_l}{t_l}+\frac{L_r}{t_r}+\frac{L_u-L_u'}{t_u}\right)-\frac{L_r^2}{t_r^2}} \tag{13}$$

$$J_3^c = 4\left(q_1F_1 + q_2F_2 + q_3F_3\right) \tag{14}$$

where q_1, q_2 and q_3 are solved according to equation (15).

$$\begin{bmatrix} \frac{L_u}{t_u}+\frac{L_r}{t_r}+\frac{L_m-L_m'}{t_m} & -\frac{L_r}{t_r} & -\frac{L_m-L_m'}{t_m} \\ -\frac{L_r}{t_r} & \frac{L_r}{t_r}+\frac{L_m'}{t_m} & -\frac{L_m'}{t_m} \\ -\frac{L_m-L_m'}{t_m} & -\frac{L_m'}{t_m} & \frac{L_l}{t_l}+\frac{L_m}{t_m} \end{bmatrix} \begin{pmatrix} q_1 \\ q_2 \\ q_3 \end{pmatrix} = \begin{pmatrix} F_1 \\ F_2 \\ F_3 \end{pmatrix} \tag{15}$$

$$J_4^c = 4\left(q_1F_1 + q_2F_2 + q_3F_3 + q_4F_4\right) \tag{16}$$

where q_1, q_2, q_3 and q_4 are solved according to equation (17).

$$\begin{bmatrix} \frac{L_u}{t_u}+\frac{L_{r1}}{t_{r1}}+\frac{L_m-L_m'}{t_m} & -\frac{L_{r1}}{t_{r1}} & -\frac{L_m-L_m'}{t_m} & 0 \\ -\frac{L_{r1}}{t_{r1}} & \frac{L_{r1}}{t_{r1}}+\frac{L_m'}{t_m} & -\frac{L_m'}{t_m} & 0 \\ -\frac{L_m-L_m'}{t_m} & -\frac{L_m'}{t_m} & \frac{L_m}{t_m}+\frac{L_{r_2}}{t_{r_2}} & -\frac{L_{r_2}}{t_{r_2}} \\ 0 & 0 & -\frac{L_{r_2}}{t_{r_2}} & \frac{L_{r_2}}{t_{r_2}}+\frac{L_l}{t_l} \end{bmatrix} \begin{pmatrix} q_1 \\ q_2 \\ q_3 \\ q_4 \end{pmatrix} = \begin{pmatrix} F_1 \\ F_2 \\ F_3 \\ F_4 \end{pmatrix} \tag{17}$$

where F_1, F_2, F_3 and F_4 denote enclosed area of each cell. L_u, L_l, L_m, L_{r_1}, L_{r_2}, L_u' and L_m' are length of each sheet, as shown in Figure 5. t_u, t_l, t_m, t_{r_1} and t_{r_2} are thickness of each sheet.

Furthermore, for a complex section with open- and close-cells, J can be expressed as

$$J = J^o + J_k^c \quad k = 1,\ 2,\ 3 \text{ and } 4 \tag{18}$$

where k represents the number of the close-cells.

In brief, the calculation process of I_y and I_z for the multi-cell sections is the same as the other types of the complex sections, but various types of the complex sections have various calculation formulations of J, as shown in Figure 5.

2.3 Simplified model of joint structure

The joint structure, formed by stamping and welding of the thin-walled plates, is a typical semi-rigid structure, which not only has the flexibility, but also has the strong stiffness. Therefore, it is necessary to apply the semi-rigid elements into the simplified frame of the BIW structure. As shown in Figure 6, the A, D, F, H and I joint structures mainly show the bending and torsional deformations. The B and C joint structures at the upper and lower ends of B-Pillar not only show the bending and torsional deformations, but also the tension deformation along the axis of B-Pillar. Especially, when the automobile carries passengers, the influence of tension at the B and C joint structures is more obvious.

However, it is difficult to analytically obtain the spring stiffness of the joint structure since the joint structure is greatly complex. The FOA utilised the detailed FE model of the joint structure to obtain its torsional and bending stiffness, and the static condensation

technique was used to reduce the DoFs (Nishigaki et al., 2001). It is worth noting that the compression and shear stiffness have a significant influence on the joint structure. Zuo et al. (2012) employed six springs to describe the deformation of the joint structure, whose stiffness is obtained from the detailed FE model of the joint structure. But, at the conceptual design stage, the detailed FE model of the joint structure cannot be determined. Therefore, this paper uses the detailed FE model of the TWB to solve the spring stiffness, which can be accurately and rapidly solved by using this method. Finally, the joint structure is simplified by using three translational and three rotational springs, as shown in Figure 7(a), and the length of each spring is zero.

Figure 6 Distributions of joints in BIW structure (see online version for colours)

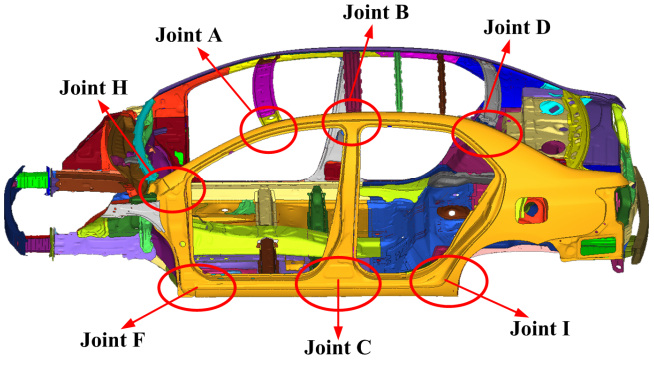

Figure 7 Semi-rigid beam and its components (see online version for colours)

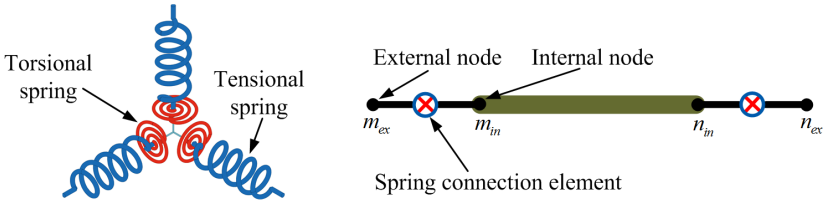

(a) Semi-rigid connection (b) Semi-rigid beam

The semi-rigid beam element is composed of one beam element and two semi-rigid elements, as shown in Figure 7(b), which has four nodes including two internal nodes and two external nodes. Figure 8(a) shows the detailed FE model of the upper structure of B-Pillar; and the corresponding simplified model, constructed by three semi-rigid beam elements, is shown in Figure 8(b).

The spring stiffness is solved by decomposing the deformation of the TWB into six types of the deformations including one axial collapse deformation, as shown in Figure 9(a), two shear deformations, as shown in Figure 10(a), two bending deformations, as shown in Figure 11(a), and one torsional deformation as shown in Figure 12(a). These deformation curves are obtained by using the CarFrame CAE software (Zuo and Bai, 2016). As long as the complex section is determined, the detailed FE model of the TWB can be automatically generated, and the constraints and loads can be also added automatically. Finally, the detailed FE model of the TWB is solved by using the Ls-dyna software.

Figure 8 Detailed model and simplified frame of the upper structure of the B-pillar (see online version for colours)

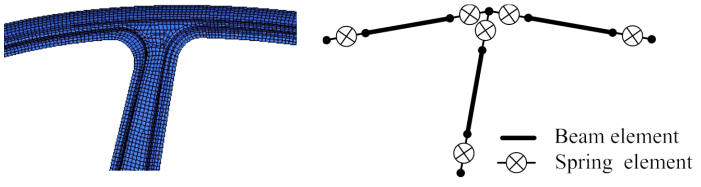

(a) Detailed model (b) Simplified model

Figure 9 Axial collapse deformation and its spring property (see online version for colours)

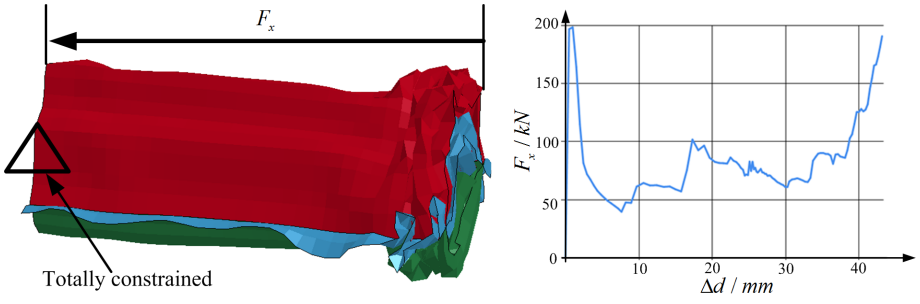

(a) Axis collapse deformation (b) Axial collapse spring property

Figure 10 Shear deformation and its spring properties (see online version for colours)

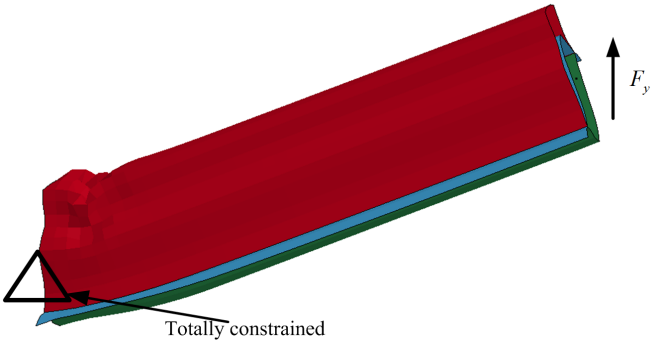

(a) Shear deformation of *y*-axis or *z*-axis

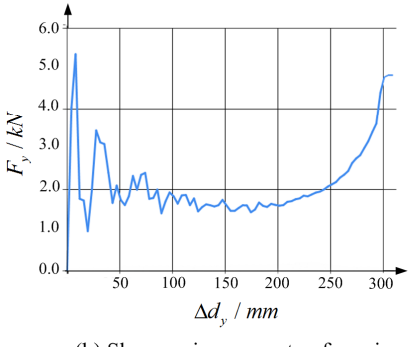

(b) Shear spring property of *y*-axis

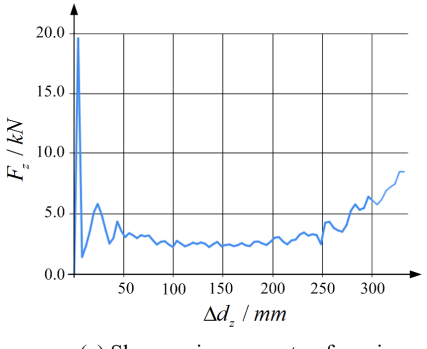

(c) Shear spring property of *z*-axis

Figure 11 Bending deformation and its spring properties (see online version for colours)

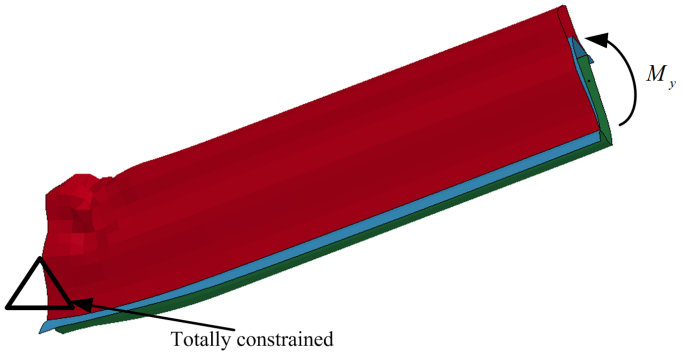

(a) Bending deformation of y-axis or z-axis

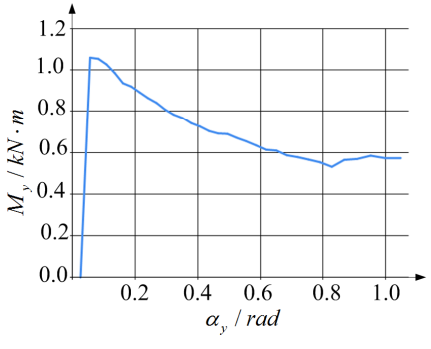

(b) Bending spring property of y-axis

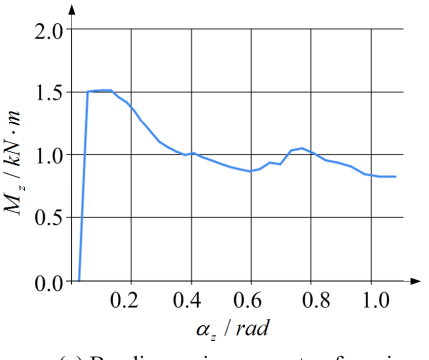

(c) Bending spring property of z-axis

Figure 12 Torsion deformation and its spring property (see online version for colours)

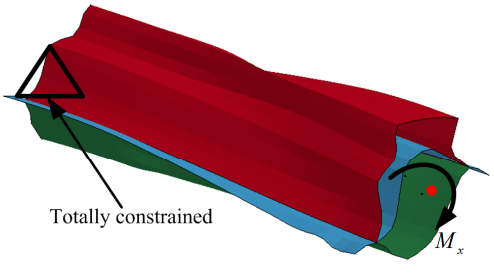

(a) Torsion deformation of x-axis

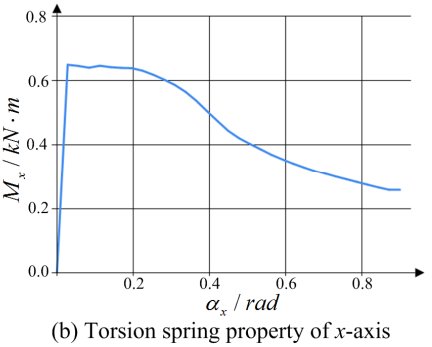

(b) Torsion spring property of x-axis

The translational and rotational spring stiffness matrix can be defined as

$$\mathbf{K}_m^i = \begin{bmatrix} r_m^i & -r_m^i \\ -r_m^i & r_m^i \end{bmatrix} \quad i = u, v, \text{ or } w, \quad \mathbf{K}_m^i = \begin{bmatrix} r_m^i & -r_m^i \\ -r_m^i & r_m^i \end{bmatrix} \quad i = x, y, \text{ or } z \tag{19}$$

The connection element stiffness matrix can be obtained by assembling these spring stiffness matrix, i.e.,

$$\mathbf{K}_m = \begin{bmatrix} r_m^u & & & & & & -r_m^u & & & & & \\ & r_m^v & & & & & & -r_m^v & & & & \\ & & r_m^w & & & & & & -r_m^w & & & \\ & & & r_m^x & & & & & & -r_m^x & & \\ & & & & r_m^y & & & & & & -r_m^y & \\ & & & & & r_m^z & & & & & & -r_m^z \\ -r_m^u & & & & & & r_m^u & & & & & \\ & -r_m^v & & & & & & r_m^v & & & & \\ & & -r_m^w & & & & & & r_m^w & & & \\ & & & -r_m^x & & & & & & r_m^x & & \\ & & & & -r_m^y & & & & & & r_m^y & \\ & & & & & -r_m^z & & & & & & r_m^z \end{bmatrix} \tag{20}$$

The beam element stiffness matrix is

$$\mathbf{K}^e = \begin{bmatrix} k_1 & & & & & & & & & & & \\ & k_2 & & & & & & & & & & \\ & & k_3 & & & & & & & & & \\ & & & k_4 & & & & \textit{Symmetry} & & & & \\ & & k_5 & & k_6 & & & & & & & \\ & k_7 & & & & k_8 & & & & & & \\ -k_1 & & & & & & k_1 & & & & & \\ & -k_2 & & & & -k_7 & & k_2 & & & & \\ & & -k_3 & & k_5 & & & & k_3 & & & \\ & & & -k_4 & & & & & & k_4 & & \\ & & k_5 & & k_9 & & & & -k_5 & & k_6 & \\ & k_7 & & & & k_{10} & & -k_7 & & & & k_8 \end{bmatrix} \tag{21}$$

where matrix elements in equation (21) can be expressed as follows

$$\begin{cases} k_1 = EA/L \\ k_2 = 12EI_z/L^3(1+\Phi_y) \\ k_3 = 12EI_y/L^3(1+\Phi_z) \\ k_4 = GI_x/L \\ k_5 = -6EI_y/L^2(1+\Phi_z) \\ k_6 = (4+\Phi_z)EI_y/(1+\Phi_z)L \\ k_7 = 6EI_z/L^2(1+\Phi_y) \\ k_8 = (4+\Phi_z)EI_z/(1+\Phi_y)L \\ k_9 = (2-\Phi_z)EI_y/L(1+\Phi_z) \\ k_{10} = (2-\Phi_y)EI_z/L(1+\Phi_y) \end{cases} \tag{22}$$

where L is length of the beam element. E and G are Young's modulus and shear modulus, respectively. $\Phi_y = 12EI_z / GA_{sy}L^2$ and $\Phi_z = 12EI_y / GA_{sz}L^2$ are shear coefficients. A_{sy} and A_{sz} denote effective shear areas.

Then, the connection element stiffness matrix $\mathbf{K}_{ij}^m$ and $\mathbf{K}_{ij}^n$ $(i=1,2; j=1,2)$, and the beam element stiffness matrix $\mathbf{K}_{ij}$ are together assembled to obtain the equilibrium equation of the semi-rigid beam element

$$\begin{bmatrix} \mathbf{K}_{11}^m & \mathbf{K}_{12}^m & & \\ \mathbf{K}_{21}^m & \mathbf{K}_{22}^m + \mathbf{K}_{11} & \mathbf{K}_{12} & \\ & \mathbf{K}_{21} & \mathbf{K}_{11}^n + \mathbf{K}_{22} & \mathbf{K}_{12}^n \\ & & \mathbf{K}_{21}^n & \mathbf{K}_{22}^n \end{bmatrix} \begin{bmatrix} \mathbf{u}_m^{ex} \\ \mathbf{u}_m^{in} \\ \mathbf{u}_n^{in} \\ \mathbf{u}_n^{ex} \end{bmatrix} = \begin{bmatrix} \mathbf{R}_m^{ex} \\ \mathbf{R}_m^{in} \\ \mathbf{R}_n^{in} \\ \mathbf{R}_n^{ex} \end{bmatrix} \tag{23}$$

where the displacement vector and load vector are defined as

$$\mathbf{u}_m^{ex} = [u_m^{ex}, v_m^{ex}, w_m^{ex}, \phi_{xm}^{ex}, \phi_{ym}^{ex}, \phi_{ym}^{ex}]^T \tag{24}$$

$$\mathbf{u}_m^{in} = [u_m^{in}, v_m^{in}, w_m^{in}, \phi_{xm}^{in}, \phi_{ym}^{in}, \phi_{ym}^{in}]^T \tag{25}$$

$$\mathbf{R}_m^{ex} = [X_m^{ex}, Y_m^{ex}, Z_m^{ex}, M_m^{ex}, M_m^{ex}, M_m^{ex}]^T \tag{26}$$

$$\mathbf{R}_m^{in} = [X_m^{in}, Y_m^{in}, Z_m^{in}, M_m^{in}, M_m^{in}, M_m^{in}]^T \tag{27}$$

The displacement vector and load vector at the n-th node need to replace subscript m by n. To reduce the pre-processing operation of the spring element modelling, a super-element is created by condensing the DoFs. Since the length of the connection element is zero, that is, the internal and external nodes coincide; the loads only act on the external nodes. Accordingly, the load vector at the internal nodes can be defined as

$$\mathbf{R}_m^{in} = [0,0,0,0,0,0]^T \text{ and } \mathbf{R}_n^{in} = [0,0,0,0,0,0]^T \tag{28}$$

Substituting equation (28) into equation (23), the second and the third line of the equation can be obtained implicitly

$$\begin{bmatrix} \mathbf{K}_{22}^m + \mathbf{K}_{11} & \mathbf{K}_{12} \\ \mathbf{K}_{21} & \mathbf{K}_{11}^n + \mathbf{K}_{22} \end{bmatrix} \begin{bmatrix} \mathbf{u}_m^{in} \\ \mathbf{u}_n^{in} \end{bmatrix} + \begin{bmatrix} \mathbf{K}_{21}^m & \mathbf{0} \\ \mathbf{0} & \mathbf{K}_{12}^n \end{bmatrix} \begin{bmatrix} \mathbf{u}_m^{ex} \\ \mathbf{u}_n^{ex} \end{bmatrix} = \begin{bmatrix} \mathbf{0} \\ \mathbf{0} \end{bmatrix} \tag{29}$$

or explicitly

$$\begin{bmatrix} \mathbf{u}_m^{in} \\ \mathbf{u}_n^{in} \end{bmatrix} = -\begin{bmatrix} \mathbf{K}_{22}^m + \mathbf{K}_{11} & \mathbf{K}_{12} \\ \mathbf{K}_{21} & \mathbf{K}_{11}^n + \mathbf{K}_{22} \end{bmatrix}^{-1} \begin{bmatrix} \mathbf{K}_{21}^m & \mathbf{0} \\ \mathbf{0} & \mathbf{K}_{12}^n \end{bmatrix} \begin{bmatrix} \mathbf{u}_m^{ex} \\ \mathbf{u}_n^{ex} \end{bmatrix} \tag{30}$$

let

$$-\begin{bmatrix} \mathbf{K}_{22}^m + \mathbf{K}_{11} & \mathbf{K}_{12} \\ \mathbf{K}_{21} & \mathbf{K}_{11}^n + \mathbf{K}_{22} \end{bmatrix}^{-1} \begin{bmatrix} \mathbf{K}_{21}^m & \mathbf{0} \\ \mathbf{0} & \mathbf{K}_{12}^n \end{bmatrix} = \begin{bmatrix} \mathbf{K}_{11}^* & \mathbf{K}_{12}^* \\ \mathbf{K}_{21}^* & \mathbf{K}_{22}^* \end{bmatrix} \tag{31}$$

then

$$\begin{bmatrix} \mathbf{u}_m^{in} \\ \mathbf{u}_n^{in} \end{bmatrix} = \begin{bmatrix} \mathbf{K}_{11}^* & \mathbf{K}_{12}^* \\ \mathbf{K}_{21}^* & \mathbf{K}_{22}^* \end{bmatrix} \begin{bmatrix} \mathbf{u}_m^{ex} \\ \mathbf{u}_n^{ex} \end{bmatrix} \tag{32}$$

Substituting equation (32) into equation (23), the DoFs at the internal nodes are condensed. The equilibrium equation of the semi-rigid beam elements at the external nodes can be written as

$$\begin{bmatrix} \mathbf{K}_{11}^m + \mathbf{K}_{12}^m \mathbf{K}_{11}^* & \mathbf{K}_{12}^m \mathbf{K}_{12}^* \\ \mathbf{K}_{21}^n \mathbf{K}_{21}^* & \mathbf{K}_{21}^n \mathbf{K}_{22}^* + \mathbf{K}_{22}^n \end{bmatrix} \begin{bmatrix} \mathbf{u}_m^{ex} \\ \mathbf{u}_n^{ex} \end{bmatrix} = \begin{bmatrix} \mathbf{R}_m^{ex} \\ \mathbf{R}_n^{ex} \end{bmatrix} \tag{33}$$

The reduced stiffness matrix has the same dimension like the stiffness matrix (21) of the beam element. Therefore, when the joint structures of the simplified frame are created, only the stiffness values of each spring are needed to input. This method greatly facilitates the pre-processing process of the joint structures.

2.4 Simplified model of plate structure

The plate structures such as the ceiling, floor and firewall not only contribute to the mass of the automobile structure, but also the stiffness. Hou et al. (2011) utilised the shell elements to build the FE model of the plate structures. However, the connection between the beam element and the shell element cannot be accurately expressed since the DoFs of the shell element and beam element are inconsistent. Therefore, in this paper, the cross beam structure is introduced to simplify the plate structure for the first time. Figure 13 shows the equivalence process from the plate structure to the cross beam structure, in which they have identical mass and central deflection. The equivalent process is described as follows.

Figure 13 Equivalence from plate structure to cross beam structure (see online version for colours)

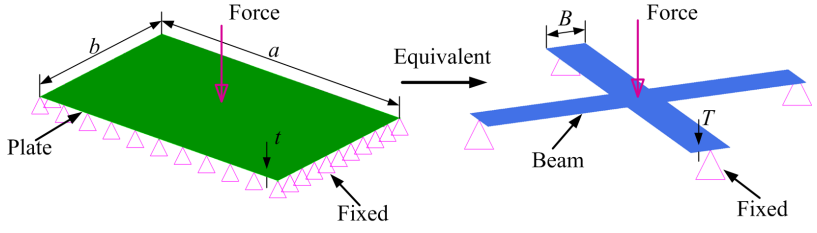

The mass of the rectangular plate structure and cross beam structure are respectively expressed as

$$m = \rho abt \tag{34}$$

$$M = \rho LBT \tag{35}$$

where ρ, a, b and t denote density, length, breadth and thickness of the plate structure, respectively. L is total length of the two diagonal beams. B and T represent breadth and thickness of each beam in the cross beam structure, respectively.

The central deflection of the rectangular plate structure and cross beam structure can be respectively obtained by

$$w = \beta Fab/D \tag{36}$$

$$W = FL^3/256\,EBT^3 \tag{37}$$

where the coefficient β is equal to 0.0056 for the fixed boundary of the plate structure. The bending stiffness D of the plate structure is equal to $Et^3/12(1-\mu^2)$.

The respective equality of the mass and central deflection between the plate structure and cross beam structure is necessary to their respective equivalence. Therefore, equations (34) and (36) should be equal to equations (35) and (37), respectively. Then, the width and thickness of the cross beam structure can be both solved as

$$B = \frac{32a^2b^2\sqrt{3\beta\left(1-\mu^2\right)}}{L^3} \tag{38}$$

$$T = \frac{L^2t}{32ab\sqrt{3\beta\left(1-\mu^2\right)}} \tag{39}$$

3 Engineering example

For the torsional loadstep, as shown in Figure 14, the DoFs of the rear suspension supports are all constrained. The moment of couple is exerted to the front suspension supports, whose force F_T is equal to 1980 N. The torsional stiffness T is defined as

$$T = \frac{F_T l'}{\theta} \tag{40}$$

$$\theta = \frac{u_2 - u_1}{l} \cdot \frac{180}{\pi} \tag{41}$$

where l' is distance between the two front suspension supports. θ is torsional angle. u_1, u_2 and l are all marked in Figure 14.

Figure 14 Torsional loadstep (see online version for colours)

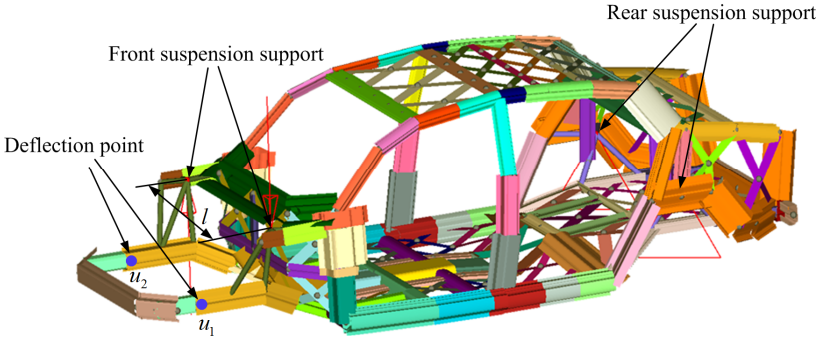

For the bending loadstep, as shown in Figure 15, the *xyz*-translational DoFs of the front suspension supports and the *z*-translational DoFs of the rear suspension supports are constrained. In the fixed places of the seats, five forces $F_B = 1670$ N are exerted to replace the weight of passengers. The bending stiffness B is defined as

$$B = \frac{5F_B}{u_{max}} \tag{42}$$

where u_{max} is the maximum displacement at the threshold beam in the *z*-axis direction.

Figure 15 Bending loadstep (see online version for colours)

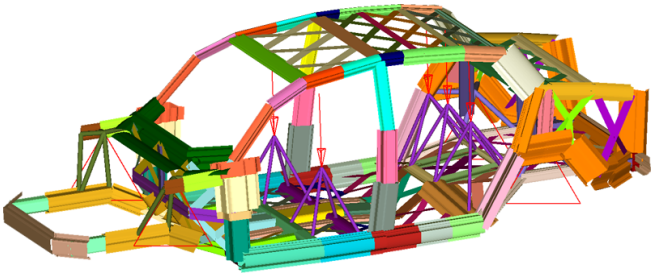

The detailed FE model of the BIW structure, solved by the Optistruct software, is regarded as a benchmarking example. To compare with the detailed FE model, two simplified frames of the BIW structure are solved by the CarFrame CAE software, as shown in Figure 16, which are created by using the rigid beam elements and the semi-rigid beam elements, respectively. All the results are listed in Table 1. The modelling cost of the simplified frame is about two days, which is much less than three months of the detailed FE model. Referring to the benchmarking detailed FE model, these two simplified frames almost acquire the same mass and centroid coordinates. However, the simplified frame with the semi-rigid beam elements obtains the more accurate torsional stiffness, bending stiffness and frequencies than the simplified frame with the rigid beam elements. Especially, compared with the detailed FE model, the errors of those evaluation indexes of the simplified frame with the semi-rigid beam elements are all controlled within 10%. The level of the accuracy can be accepted at the conceptual design stage.

Figure 16 CarFrame CAE software (see online version for colours)

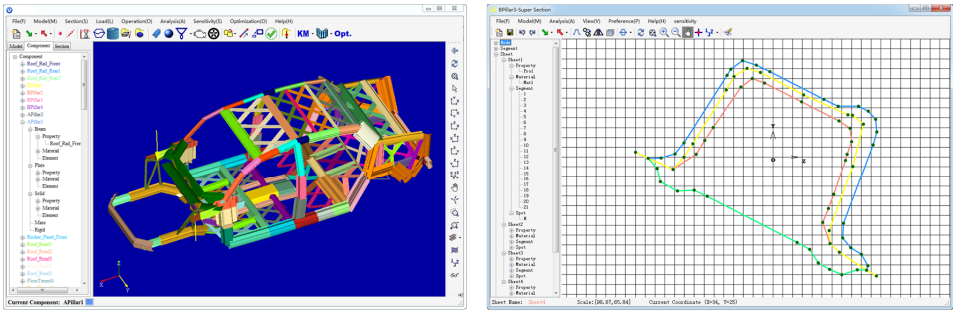

(a) CarFrame (b) SuperSection

Table 1 Comparison of torsional stiffness, bending stiffness and frequency

Evaluation indexes		*BIW*				
		Detailed	*Simplified frame with rigid beams*	*Error (%)*	*Simplified frame with semi-rigid beams*	*Error (%)*
Mass (kg)		263.7	263.7	0.00%	263.7	0.00%
Centroid coordinates (mm)	*x*	–2223.9	–2224.0	0.00%	–2224.0	0.00%
	y	3.8	0.0	0.00%	0.0	0.00%
	z	619.6	619.7	0.01%	619.7	0.01%
Torsional stiffness (N·m/°)		7418	22743	206.59%	7966	7.39%
Bending stiffness (N/m)		17996	30547	69.74%	16540	8.09%
Frequency (Hz)	1st	28.6	45.5	59.09%	26.2	8.39%
	2nd	35.5	61.3	72.68%	38.3	7.89%
	3rd	52.0	65.8	26.54%	49.2	5.38%

4 Conclusions

The aim of this paper is to propose a rapid and accurate modelling method of the simplified frame, which can accelerate the conceptual design of the BIW structure. The conclusions can be summarised as follows:

1 The TWBs with the complex sections, semi-rigid elements and cross beam structures can be together used to rapidly and accurately create the simplified frame of the BIW structure, which can be easily designed and modified for the development of the new automobile structure.

2 Numerical example demonstrates that the simplified frame with the semi-rigid beam elements can obtain the more accurate torsional stiffness, bending stiffness and frequencies than the simplified frame with the rigid beam elements. Especially, the errors of those evaluation indexes are all controlled within 10%. The level of the accuracy can be accepted at the conceptual design stage.

3 The proposed modelling methods can be implemented by using the CarFrame CAE software, which shortens the modelling cycle of the BIW structure within one or two days.

4 Next, the crashworthiness design of the simplified frame with the semi-rigid beam elements will be investigated for the conceptual design of the automobile structure.

Acknowledgements

The work was supported by the Plan for Scientific and Technological Development of Jilin Province (Grant No. 20210101058JC).

References

Bai, J., Li, Y. and Zuo, W. (2017) 'Cross-sectional shape optimisation for thin-walled beam crashworthiness with stamping constraints using genetic algorithm', *International Journal of Vehicle Design*, Vol. 73, Nos. 1–3, pp.76–95.

Bai, J., Meng, G., Wu, H. and Zuo, W. (2019a) 'Bending collapse of dual rectangle thin-walled tubes for conceptual design', *Thin-Walled Structures*, Vol. 135, pp.185–195.

Bai, J., Meng, G. and Zuo, W. (2019b) 'Rollover crashworthiness analysis and optimization of bus frame for conceptual design', *Journal of Mechanical Science and Technology*, Vol. 33, No. 7, pp.3363–3373.

Bai, J. and Zuo, W. (2020) 'Hollow structural design in topology optimization via moving morphable component method', *Structural and Multidisciplinary Optimization*, Vol. 61, No. 1, pp.187–205.

Chen, W. and Zuo, W. (2014) 'Component sensitivity analysis of conceptual vehicle body for lightweight design under static and dynamic stiffness demands', *International Journal of Vehicle Design*, Vol. 66, No. 2, pp.107–123.

Donders, S., Takahashi, Y., Hadjit, R., Van Langenhove, T., Brughmans, M., Van Genechten, B. and Desmet, W. (2009) 'A reduced beam and joint concept modeling approach to optimize global vehicle body dynamics', *Finite Elements in Analysis and Design*, Vol. 45, No. 6, pp.439–455.

Gui, C., Bai, J. and Zuo, W. (2018) 'Simplified crashworthiness method of automotive frame for conceptual design', *Thin-Walled Structures*, Vol. 131, pp.324–335.

Hamza, K. and Saitou, K. (2004) 'Design optimization of vehicle structures for crashworthiness using equivalent mechanism approximations', *Journal of Mechanical Design*, Vol. 127, No. 3, pp.485–492.

Hou, W., Shan, C. and Zhang, H. (2015) 'Multi-level optimization method for vehicle body in conceptual design', *ASME 2015 International Design Engineering Technical Conferences and Computers and Information in Engineering Conference Paper*, Boston, Massachusetts, USA, p.V003T01A023, doi: 10.1115/DETC2015-48034.

Hou, W., Zhang, H., Zhang, W. and Hu, P. (2011) 'Rapid structural property evaluation system for car body advanced design', *International Journal of Vehicle Design*, Vol. 57, Nos. 2–3, pp.242–253.

Huang, G., Wang, H., Gao, G. and Li, G. (2011) 'Modified combined approximations and the application in reanalysis of vehicle frame stiffness', *Journal of Mechanical Engineering*, Vol. 47, No. 18, pp.86–92.

Huang, G., Wang, H. and Li, G. (2015) 'Some modifications for ES-FEM and its application for vehicle design', *Engineering Computations*, Vol. 32, No. 5, pp.1432–1459.

Lyu, N., Lee, B. and Saitou, K. (2006) 'Optimal subassembly partitioning of space frame structures for in-process dimensional adjustability and stiffness', *Journal of Mechanical Design*, Vol. 128, No. 3, pp.527–535.

Lyu, N. and Saitou, K. (2006) 'Decomposition-based assembly synthesis of space frame structures using joint library', *Journal of Mechanical Design*, Vol. 128, No. 1, pp.57–65.

Mohsin, M.E. and Sadek, E.A. (1980) 'On the dynamics of plates using a beam-analog', *Computers and Structures*, Vol. 12, No. 3, pp.267–272.

Mundo, D., Donders, S., Stigliano, G. and Auweraer, H.V.D. (2011) 'Concept design of vehicle bodies using reduced models of beams, joints and panels', *International Journal of Vehicle Design*, Vol. 57, No. 1, pp.71–83.

Nakagawa, T., Nishigaki, H., Tsurumi, Y. and Kikuchi, N. (2004) *First Order Analysis for Automotive Body Structure Design – Part 4: Noise and Vibration Analysis Applied to a Subframe*, SAE Technical Paper, doi: 10.4271/2004-01-1661.

Nikolaidis, E. and Lee, K. (1992) *A 3-D Joint Model for Automotive Structures*, SAE Technical Paper, doi: 10.4271/921088.

Nishigaki, H. (2002) 'First order analysis for automotive body structure design using excel', *R & D Review of Toyota CRDL*, Vol. 37, No. 1, pp.1–8.

Nishigaki, H., Amago, T., Sugiura, H., Kojima, Y., Nishiwaki, S. and Kikuchi, N. (2004) *First Order Analysis for Automotive Body Structure Design – Part 1: Overview and Applications*, SAE Technical Paper, doi: 10.4271/2004-01-1658.

Nishigaki, H. and Kikuchi, N. (2004) *First Order Analysis for Automotive Body Structure Design – Part 3: Crashworthiness Analysis Using Beam Elements*, SAE Technical Paper, doi: 10.4271/2004-01-1660.

Nishigaki, H., Nishiwaki, S., Amago, T., Kojima, Y. and Kikuchi, N. (2001) *First Order Analysis – New CAE Tools for Automotive Body Designers*, SAE Technical Paper, doi: 10.4271/2001-01-0768.

Overhagh, W.H. (1995) *Use of Aluminum in Automotive Space Frame*, SAE Technical Paper, doi: 10.4271/950721.

Shahhosseini, A.M., Prater, G., Osborne, G.M., Kuo, E.Y. and Mehta, P.R. (2010) 'Major compliance joint modelling survey for automotive body structures', *International Journal of Vehicle Systems Modelling and Testing*, Vol. 5, No. 1, pp.1–17.

Suh, M., Suhr, J. and Yang, W. (2002) 'Condensed joint matrix method for the joint structure of a vehicle body', *Proceedings of the Institution of Mechanical Engineers, Part D: Journal of Automobile Engineering*, Vol. 216, No. 1, pp.35–41.

Timoshenko, S. and Goodier, J.N. (1951) *Theory of Elasticity,* 2nd ed., McGraw-Hill Book Company, New York.

Torstenfelt, B. and Klarbring, A. (2007) 'Conceptual optimal design of modular car product families using simultaneous size, shape and topology optimization', *Finite Elements in Analysis and Design*, Vol. 43, No. 14, pp.1050–1061.

Wang, H., Li, G. and Li, E. (2010) 'Time-based metamodeling technique for vehicle crashworthiness optimization', *Computer Methods In Applied Mechanics and Engineering*, Vol. 199, No. 37, pp.2497–2509.

Yoshimura, M., Nishiwaki, S. and Izui, K. (2005) 'A multiple cross-sectional shape optimization method for automotive body frames', *Journal of Mechanical Design*, Vol. 127, No. 1, pp.49–57.

Zuo, J. (2013) 'An object-oriented graphics interface design and optimization software for cross-sectional shape of automobile body', *Advances in Engineering Software*, Vol. 64, pp.1–10.

Zuo, W. (2015) 'Bi-level optimization for the cross-sectional shape of a thin-walled car body frame with static stiffness and dynamic frequency stiffness constraints', *Proceedings of the Institution of Mechanical Engineers Part D Journal of Automobile Engineering*, Vol. 229, No. 8, pp.1046–1059.

Zuo, W. and Bai, J. (2016) 'Cross-sectional shape design and optimization of automotive body with stamping constraints', *International Journal of Automotive Technology*, Vol. 17, No. 6, pp.1003–1011.

Zuo, W., Li, W., Xu, T., Xuan, S. and Na, J. (2012) 'A complete development process of finite element software for body-in-white structure with semi-rigid beams in. NET framework', *Advances in Engineering Software*, Vol. 45, No. 1, pp.261–271.

Zuo, W., Lu, Y., Zhao, X. and Bai, J. (2018) 'Cross-sectional shape design of automobile structure considering rigidity and driver's field of view', *Advances in Engineering Software*, Vol. 115, pp.161–167.

Zuo, W. and Saitou, K. (2017) 'Multi-material topology optimization using ordered SIMP interpolation', *Structural and Multidisciplinary Optimization*, Vol. 55, No. 2, pp.477–491.

Zuo, W., Xu, T., Zhang, H. and Xu, T. (2011) 'Fast structural optimization with frequency constraints by genetic algorithm using adaptive eigenvalue reanalysis methods', *Structural and Multidisciplinary Optimization*, Vol. 43, No. 6, pp.799–810.

Zuo, W., Yu, J. and Saitou, K. (2016) 'Stress sensitivity analysis and optimization of automobile body frame consisting of rectangular tubes', *International Journal of Automotive Technology*, Vol. 17, No. 5, pp.843–851.